Elasticity and thermal transport of commodity plastics

Céline Ruscher,[1,2] Jörg Rottler,[1,2] Charlotte E. Boott,[3] Mark J. MacLachlan,[1,3] and Debashish Mukherji[1,*]
[1]*Stewart Blusson Quantum Matter Institute, University of British Columbia, Vancouver, Canada BC V6T 1Z4*
[2]*Department of Physics and Astronomy, University of British Columbia, Vancouver, Canada BC V6T 1Z1*
[3]*Department of Chemistry, University of British Columbia, Vancouver, Canada BC V6T 1Z1*

(Received 10 October 2019; published 16 December 2019)

Applications of commodity polymers are often hindered by their low thermal conductivity. In these systems, going from the standard polymers dictated by weak van der Waals interactions to biocompatible hydrogen-bonded smart polymers, the thermal transport coefficient κ varies between 0.1 and 0.4 $\mathrm{Wm^{-1}K^{-1}}$. Combining all-atom molecular dynamics simulations with some experiments, we study thermal transport and its link to the elastic response of (standard and smart) commodity plastics. We find that there exists a maximum attainable stiffness (or sound-wave velocity), thus providing an upper bound of κ for these solid polymers. The specific chemical structure and the glass transition temperature play no role in controlling κ, especially when the microscopic interactions are hydrogen-bonding based. Our results are consistent with the minimum thermal conductivity model and existing experiments. The effect of polymer stretching on κ is also discussed.

DOI: 10.1103/PhysRevMaterials.3.125604

I. INTRODUCTION

In crystals, the periodicity of the crystal lattice allows for the propagation of vibrational excitations (or phonons) that carry a heat current. Here the coefficient of thermal conductivity κ is directly related to the heat capacity c, the phonon mean-free path Λ, and the group velocity v_g [1,2]. Most commonly known crystals have $\kappa \gtrsim 100$ $\mathrm{Wm^{-1}K^{-1}}$ [3], which can even exceed 1000 $\mathrm{Wm^{-1}K^{-1}}$ in carbon-based materials [4–7]. On the other hand, $\Lambda \to 0$ for disordered (amorphous) materials, leading to $\kappa < 10$ $\mathrm{Wm^{-1}K^{-1}}$ [8]. These materials are broadly classified as hard matter having large cohesive energy densities. Moreover, these systems often require rather cumbersome materials processing, can be expensive, and often have restrictive flexibility. In this context, another class consists of polymers that also form an amorphous state. Broadly speaking, polymers are classified as soft matter where the relevant energy scale is comparable to the thermal energy k_BT with temperature $T = 300$ K and k_B being the Boltzmann constant [9]. Therefore, the properties of polymers are dictated by large fluctuations and thus are highly flexible, easily processable, and most times inexpensive.

The polymers are materials that provide a suitable platform for the flexible design of advanced functional materials [10–15]. Moreover, solvent free (dry) amorphous states of common polymers, often referred to as commodity plastics, usually have rather small $\kappa < 0.5$ $\mathrm{Wm^{-1}K^{-1}}$ [16–22]. While small κ values are extremely desirable for thermoelectric materials [23,24], they also create severe problems when used under high-temperature conditions for electronic packaging, organic solar cells, and organic light emitting diodes, to name a few [25,26].

The properties of commodity plastics, such as polyethylene (PE), polystyrene (PS), and/or poly(methyl methacrylate) (PMMA), are dictated by weak van der Waals (vdW) interactions resulting in $\kappa < 0.2$ $\mathrm{Wm^{-1}K^{-1}}$ [16,19]. These polymers are water insoluble because of their dominant carbon-based (hydrophobic) architectures. The bonded interactions in these polymers are based on carbon-carbon covalent bonds, having a bond strength of $80\,k_BT$ [27], and thus live forever under unperturbed conditions, creating severe environmental problems. Therefore, recent interest has been directed toward peptide-based polymers that are biocompatible/biodegradable and are often referred to as commodity "smart" polymers. These systems are also water soluble because of their dominant hydrogen (H) bonds [10,13,14]. The dry states of these H-bond-based polymers usually have $\kappa \sim 0.3$–0.4 $\mathrm{Wm^{-1}K^{-1}}$ [18,19,22].

The thermal conductivity of these commodity plastics has a rather restrictive tunability limiting their broad applications. Traditionally, extensive efforts have been devoted to tune κ of polymers by nanomaterials blending [26,28–30]. Other strategies include polymer blending, cross linking, and macromolecular engineering [18,19,22,31]. Advances are usually carried from the experimental side with several carefully conducted works, while simulation efforts are rather limited [17,20,22,31–35]. The majority of these simulation efforts deal with vdW-based polymers.

In this work, we use large-scale all-atom molecular dynamics simulations to relate microscopic molecular organization, propensity of forming hydrogen bonds, and mechanical response and its links to the thermal transport of solid macromolecular systems. For this purpose, we have chosen a set of six different linear (co-)polymers in their solvent-free (dry) states: namely PMMA, poly(*N*-acryloyl piperidine) (PAP), poly(acrylic acid) (PAA), polyacrylamide (PAM), poly(*N*-isopropyl acrylamide) (PNIPAM), and copolymer P(AM-co-NIPAM) at 20% AM monomer mole fraction. The schematic

*debashish.mukherji@ubc.ca

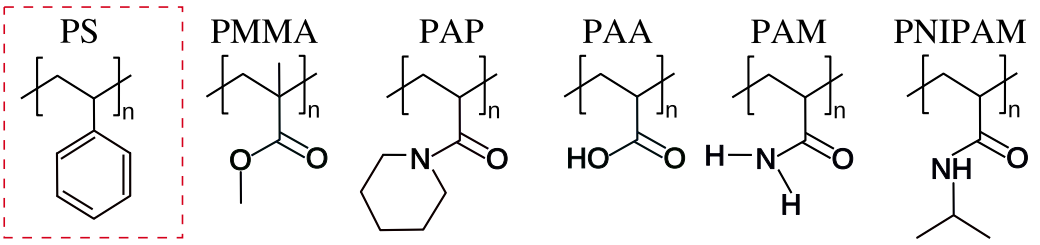

FIG. 1. Schematics showing different monomeric structures investigated in this study: poly(styrene) (PS), poly(methyl methacrylate) (PMMA), poly(*N*-acryloyl piperidine) (PAP), poly(acrylic acid) (PAA), poly(acrylamide) (PAM), poly(*N*-isopropyl acrylamide) (PNIPAM), and copolymer P(AM-co-NIPAM) at 20% AM monomer mole fraction. We have simulated chains of all these systems except for PS. For PS we discuss experimental and simulation data from the published literature only.

representation of monomer structures of all these polymers are shown in Fig. 1. We have chosen these particular polymeric systems because of their experimental relevance [19]. Furthermore, while the properties of PAP and PMMA are dictated by pure vdW interactions and for PAM and PAA pure H bonds are dominant, we have also chosen two additional systems, namely PNIPAM and P(AM-co-NIPAM), where the delicate balance between H bonds and vdW interactions plays a key role (see Sec. III B for more details). For comparison, we have also reanalyzed simulation data of H-bonded asymmetric PAA-PAM blends obtained in our earlier work [22]. Experiments are also performed for pure PNIPAM, where experimental data were not available. Our analysis suggests that there is a maximum in attainable κ for commodity plastics, which can be attributed to the maximum in materials stiffness and is consistent with the minimum thermal conductivity model [8].

The remainder of the paper is organized as follows: In Sec. II, we sketch our methodology. Results and discussions are presented in Sec. III and finally we draw our conclusions in Sec. IV.

II. METHOD, MODEL, AND MATERIALS

A. Molecular dynamics simulations

The GROMACS molecular dynamics package is used for the initial equilibration of different polymers in their (solvent free) melt states at $T = 600$ K [36]. These equilibrated samples are subsequently quenched down to $T = 300$ K where thermal transport calculations are performed using the LAMMPS molecular dynamics package [37].

The initial equilibration in GROMACS is performed in the isobaric ensemble, where the temperature is imposed using the Berendsen thermostat with a coupling constant of 2 ps and the pressure is set to 1 bar with a Berendsen barostat with a coupling time of 0.5 ps [38]. Electrostatics are treated using the particle-mesh Ewald method [39]. The interaction cutoff for nonbonded interactions is chosen as 1.0 nm. The simulation time step is chosen as $\triangle t = 1$ fs and the equations of motion are integrated using the leap-frog algorithm [40]. All bond vibrations are constrained using the LINCS algorithm [41].

A polymer chain length of $N_\ell = 30$ monomers was chosen for PMMA, PAP, PAA, and PAM, while $N_\ell = 32$ is taken for PNIPAM and P(NIPAM-co-AM). Note that the latter two systems have slightly larger N_ℓ because these configurations are taken from our earlier works [15,22,42]. These chains are typically 12–15 ℓ_p, with ℓ_p being the persistence length. Chains are placed randomly in a cubic simulation box where the equilibrated linear dimensions L vary between 7.7 and 8.3 nm. Simulations are performed for 80 ns at $T = 600$ K. This time is around one order of magnitude larger than the longest relation time for all polymers investigated herein.

The standard OPLS force field [43] is used to simulate all polymers except for PMMA and PAM. For PMMA [15] and PAM [42], we have taken the modified force-field parameters used earlier to study single-chain conformations in aqueous solutions. To ensure that these force-field parameters can also capture properties of solid polymeric materials, we have calculated the glass transition temperatures T_g for all six polymers, see Table I. Calculated T_g values in our simulations and its comparison to the experimental data are listed in Table I. Note that while the measured value of T_g for PNIPAM is obtained in our experiments, the other values are taken from the published literature [18,27].

We employ the nonequilibrium method to calculate κ [45]. In this method, a heat flux J through the material is generated in microcanonical ensemble by swapping atomic velocities between the hot $T_{\rm hot}$ and the cold $T_{\rm cold}$ region of the simulation box (see the inset of Fig. 2). For this purpose the simulation cell is subdivided into 20 slabs along the z axis. Velocity swapping was performed between the slowest atom in the center slab (see the red region in the inset of

TABLE I. Glass transition temperatures T_g of different polymers shown in Fig. 1. Available experimental data are also compiled for comparison. Note that we have obtained T_g value for PNIPAM in our experiments, see Supplemental Material Sec. SI for more details [44].

Polymer	T_g (K)	$T_g^{\rm exp}$ (K)
PMMA	390	378 [27]
PAP	387	380 [18]
PAA	400	385 [18]
PAM	445	430 [27]
PNIPAM	421	413
P(NIPAM-co-AM)	455	—
PS	—	373 [27]

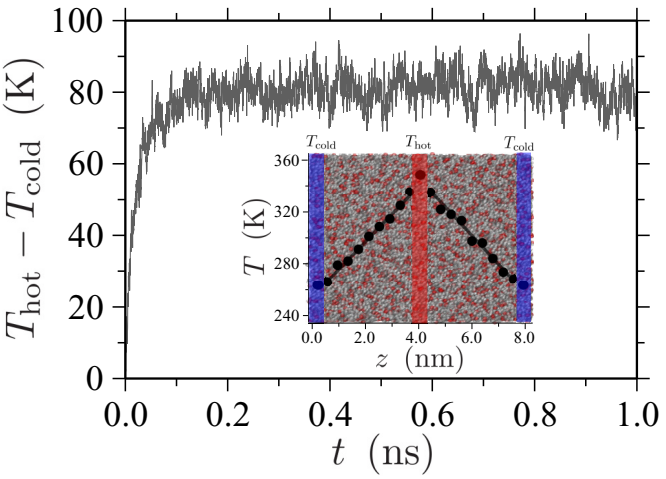

FIG. 2. The main panel shows time equilibration of the temperature difference between the hot (T_{hot}) and the cold (T_{cold}) regions of a solid PMMA material. In the inset we show the steady-state temperature profile along the z axis. To establish the temperature gradient, the simulation domain is subdivided into 20 slabs with equal width. Within this setup, each slab typically contains ∼3000 atoms.

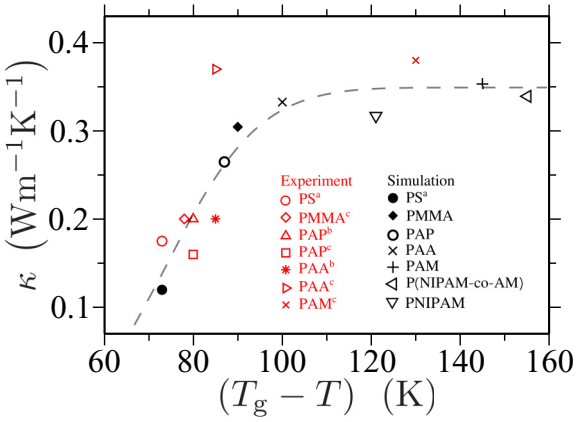

FIG. 3. Thermal transport coefficient κ as a function of the distance from the glass transition temperature ($T_g - T$). The data are shown for a temperature $T = 300$ K. Calculated κ values are compared with the available experimental data for several polymeric systems (as shown in Fig. 1). Data for *a*, *b*, and *c* are taken from Refs. [17], [18], and [19], respectively. Typical errors of 5 − 10% are estimated from four different κ calculations for each polymeric system using different random seeds during microcanonical simulations. Line is drawn to guide the eye.

Fig. 2) and the fastest atom in the slab at the cell boundary (see the blue regions in the inset of Fig. 2). This swapping was performed every 40 fs with a time step $\triangle t = 0.2$ fs. The system is initially equilibrated for 1 ns when the steady state of temperature difference between hot and cold regions is obtained, as shown in the main panel of Fig. 2. After the steady state is reached, J was then calculated for another 0.1 ns simulation. A linear fit of the temperature profile as a function of z coordinate (see the inset of Fig. 2) is used to calculate the thermal transport coefficient κ using Fourier's law of heat conduction, i.e., $\kappa = J/|\triangle T/\triangle z|$.

B. Polymer synthesis

To validate the ability of force-field parameters of PNIPAM to reproduce properties of dry states, we have also synthesized a PNIPAM sample using the reversible addition-fragmentation chain-transfer polymerization following the exact protocol discussed earlier for PNIPAM [46]. The T_g of this sample is measured using differential scanning calorimetry (DSC), see Supplemental Fig. S2 [44]. As seen from Table I, measured and calculated values of T_g for PNIPAM are in very good agreement. Note that given the fact that both PAM and PNIPAM force fields are well validated, we expect to have reasonably captured the properties of solid copolymers with these two constituents. Therefore, we abstain from synthesizing a P(NIPAM-co-AM) system.

III. RESULTS AND DISCUSSIONS

A. Thermal conductivity, elasticity, and glass transition temperature

We start our discussion by investigating the effect of T_g on κ for different solid polymers. In Fig. 3 we show a comparative plot of κ from our simulations and the corresponding experimental values from the published literature. It can be seen that κ first increases up to $(T_g - T) \simeq 100$ K, i.e., dry polymers where the properties are dictated by weak vdW interactions. For $(T_g - T) \geqslant 100$ K, κ values almost remain constant with T_g. These are H-bonded polymers. It can be seen that the overall trend in the variation of κ for different polymers follows a reasonable master curve, with a couple of exceptions. For example, the experimental κ values for PAA between two experiments [18,19] deviate by a factor of two, while these individual experiments report typical error bars of about 5%. In this context, we find that our calculated κ for PAA is closer to the data reported in Ref. [19]. However, our calculated κ for PMMA is overestimated in comparison to experiments [19]. It is also important to investigate why κ remains invariant with T_g for H-bonded polymers and not for vdW-based systems. For this purpose, we need to look more closely into the microscopic interactions governing the glass forming behavior of these commodity plastics.

To investigate the relationship among T_g, microscopic interactions, and κ, we have first calculated the average number of H bonds between nonbonded monomers. An H bond is calculated using the standard GROMACS subroutine, where an H bond exists when the donor-acceptor distance is $\leqslant$0.35 nm and the acceptor-donor-hydrogen angle is $\leqslant 30^\circ$. In Table II we show the H bond for three different systems, which span the full range 100 K $< (T_g - T) <$ 160 K, where κ remain invariant (see Fig. 3). By comparing PAA and PAM data, we find that PAM has almost twice the number of H bonds in comparison to PAA (see column two in Table II). This is not surprising given that PAM monomers have twice as many possibilities of forming H bonds than PAA (see column three in Table II and corresponding monomer structures in Fig. 1). Furthermore, a higher number of H bonds also leads to stronger interactions. For example, considering that the H-bond strength is between 4 and 8 k_BT, the energy

TABLE II. Average number of hydrogen bonds (H bonds) between nonbonded monomers for three different polymeric systems. Data are shown for a temperature $T = 300$ K. For comparison we have also listed the maximum number of possible H bonds between two nonbonded monomers.

Polymer	H bond	Max H bond
PAA	0.71	2.0
PAM	1.41	4.0
PNIPAM	0.51	2.0

per contact for PAM can be $\simeq 10\,k_BT$, while this is $\simeq 5\,k_BT$ for PAA. This trend is consistent with an almost 50 K increase in T_g for PAM in comparison to PAA (see Table I). Note that the contacts in these systems originate because of the interdigitation of the side groups, leading to H bonds.

It is not that H bonds are always the dominant interactions in a system and vdW interactions can be completely ignored. Here PNIPAM is an interesting system, while PNIPAM has fewer H bonds than PAA (see Table II) and PNIPAM still has a higher T_g (see Table I). This trend can be understood from the chemical structure of a NIPAM monomer that not only has the hydrophilic amide moiety but also has a rather large hydrophobic isopropyl group (see the PNIPAM structure in Fig. 1). Here the interaction between two carbon atoms of different isopropyl groups, belonging to two nonbonded monomers, can be estimated by using the Boltzmann inversion of the pair distribution function $g(r)$. The carbon-carbon potential-of-mean-force can then be estimated using $V(r) = -k_BT \ln[g(r)]$ [47]. It can be seen from Fig. 4 that while two carbon atoms only interact by about $V(r) \simeq k_BT/2$, collectively can lead to $>5\,k_BT$ interaction strength. This is because one carbon atom in an isopropyl group can have as many as 8–10 neigboring carbons. Therefore, the vdW interactions between isopropyl groups also give an almost similar contribution to the contact energy and thus to the T_g for PNIPAM. Note that because of this delicate balance between vdW and H-bonded interactions in PNIPAM, we will investigate this system in more details at a later stage of this manuscript.

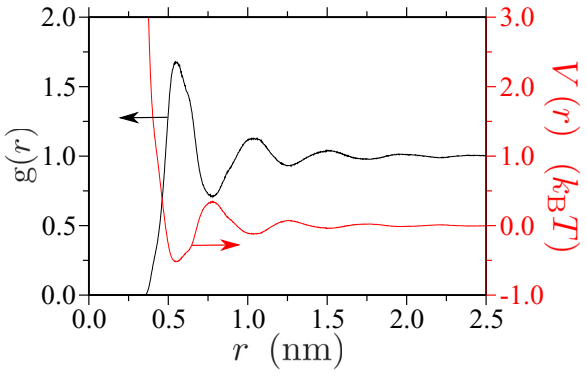

FIG. 4. Radial distribution function $g(r)$ and potential of mean force $V(r) = -k_BT \ln[g(r)]$ for a PNIPAM system at $T = 300$ K. Data are calculated between carbon atoms of the PNIPAM isopropyl group. Arrows direct at the corresponding y axes.

The discussion in the preceding two paragraphs presents a consistency check between monomer structures, H bond and T_g. However, it still remains counterintuitive that κ almost remains invariant (i.e., $\sim$0.32 $\mathrm{Wm^{-1}K^{-1}}$) even when T_g increases. Generally speaking, T_g is related to material stiffness, i.e., a material with higher T_g also exhibits higher stiffness. Therefore, it is worthwhile to investigate the relationship between the elastic response of different polymeric systems and its relationship with κ. In this context, it is well known that κ is directly related to the elasticity of materials. A simple estimate for the lower bound of the thermal conductivity $\kappa^{\min}$, referred to as the minimum thermal conductivity model, relates to the sound-wave velocities (or the materials stiffness) using the expression [8,19,48]

$$\kappa^{\min} = \left(\frac{\pi}{48}\right)^{1/3} k_B n^{2/3} (v_\ell + 2v_t), \tag{1}$$

where n is the atomic number density and $v_l = \sqrt{C_{11}/\rho}$ and $v_t = \sqrt{C_{44}/\rho}$ are the longitudinal and transverse sound-wave velocities, respectively. Here $C_{11} = K + 4C_{44}/3$, C_{44} is the shear modulus, K is the bulk modulus, and ρ is the mass density. We use volume fluctuations to calculate K from NpT simulations using the expression

$$K = k_BT \frac{\langle V \rangle}{\langle V^2 \rangle - \langle V \rangle^2} \tag{2}$$

and this also leads to

$$C_{44} = \frac{3K(1-2\nu)}{2(1+\nu)}, \tag{3}$$

with ν being the Poisson's ratio; ν is calculated from the isobaric uniaxial stretching of different samples, which was performed at a strain rate of 10^{-7} $\mathrm{fs^{-1}}$ and at $T = 300$ K. Details of the elastic constants and ν for different systems are listed in the Supplemental Table SII [44]. Note that Eqs. (2) and (3) are good estimators when dealing with isotropic systems. For anisotropic systems, individual components of the elasticity tensor should be separately calculated.

As predicted by Eq. (1), κ is related to C_{44} and C_{11}. Therefore, we will now investigate the variation of elastic moduli for different systems. Note that while both C_{44} and C_{11} have very similar behavior with T_g for different systems, see Supplemental Tables SII and SIII [44], here we only plot C_{44} to explain the trend underlying microscopic picture. Therefore, in Fig. 5 we show C_{44} as a function of scaled T_g. Consistent with the trend in Fig. 3 we find that C_{44} remains constant for $(T_g - T) > 100$ K, i.e., H-bonded systems. In this context, it is important to mention that all our systems are investigated at least 80 K below their T_g, such that their elastic moduli are already in the glassy plateau of the sigmoidal curve. Therefore, these systems can be treated within the harmonic approximation. Since the mechanical response is dictated by small (local) particle fluctuations, the corresponding elastic constants are then given by the curvature of the potential energy surface around the equilibrium particle positions. Ideally speaking, the high-dimensional potential energy surface of a macromolecular amorphous system is extremely complex. Microscopically, however, this complex energy surface can be decomposed into different contributions. In the case when H bonds play a significant role in

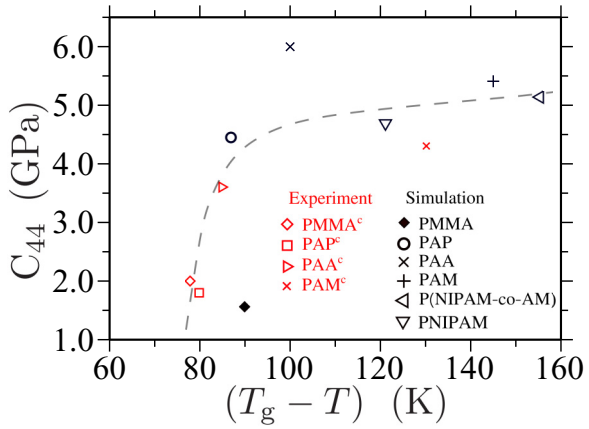

FIG. 5. Shear modulus C_{44} as a function of the distance from the glass transition temperature $(T_g - T)$ for different dry polymer systems. Data are shown for a temperature of $T = 300$ K. Typical errors of ∼20% are estimated from four different calculations for each polymeric system. Experimental data c are taken from Ref. [19]. Line is drawn to guide the eye.

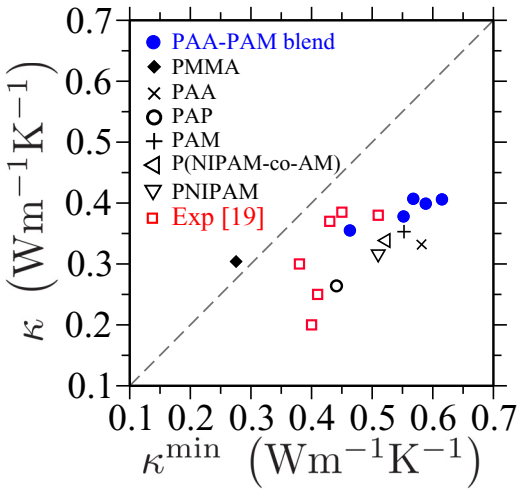

FIG. 6. Calculated thermal transport coefficients κ as a function of $\kappa^{\min}$ obtained using Eq. (1). Dashed line is a linear law with zero intercept and unity slope. Data are shown for dry states of six different linear polymer systems and also for the PAM-PAA blends [22]. For comparison, we have also included data from the published experimental literature [19]. Note that we have used $n_c = 2(n - n_H)/3$ instead of n in Eq. (1) with n_H being the density of H-atoms, see the text for more details.

dictating properties of commodity plastics, the stiffness is related to the particle fluctuations around their typical H-bond length of 0.34 nm. Furthermore, an H bond is inherently directional and restrictively local in nature. Note that locality of an H bond originates because, when an oxygen atom forms a bond with a hydrogen, the same hydrogen atom involved in this pair cannot simultaneously interact with another oxygen via an H bond. Furthermore, because of the dense packing of side chains, even individual oxygen atoms can only form a maximum of one H bond. While these bonds dynamically break and form, instantaneously these are strictly restricted between a pair of particles. Therefore, so long as interactions are H-bond dominated, materials stiffness remains invariant irrespective of the specific monomer structure.

When the microscopic interactions are predominantly vdW based, such as PMMA, PAP, or PS, each atom experiences an effective interaction due to the presence of all other particles within the first neigboring shell. This effectively depends on the monomer architecture and their chemical constituents and thus can alter the contact energy density, T_g, and also the stiffness, see data for $(T_g - T) < 100$ K in Fig. 5. However, the plateaus observed in κ and C_{44} for H-bonded systems within the range 100 K $< (T_g - T) <$ 160 K (see Figs. 3 and 5) also suggest that there exists a restrictive range of κ for the H-bonded plastics, i.e., 0.3 Wm^{-1}K^{-1} $< \kappa \leqslant$ 0.4 Wm^{-1}K^{-1}. Furthermore, this maximum in κ is independent of specific chemical structure of a monomer and T_g.

B. Thermal conductivity, elasticity, and minimum thermal conductivity model

We will now compare our simulation data with the minimum thermal conductivity model presented in Eq. (1) [8]. For this purpose, we have calculated v_ℓ and v_t in our simulations. These values and corresponding elastic moduli are presented in the Supplemental Tables SII and SIII [44]. In Fig. 6 we show κ from simulations as a function of $\kappa^{\min}$. Data are shown for six different polymers investigated in this study, reanalysis of our earlier published simulation work of H-bonded polymer blends [22], and the available experimental data [19]. It can be seen that κ and $\kappa^{\min}$ values show a reasonable correlation. Furthermore, a slight overestimation of $\kappa^{\min}$ in all cases is due to the fact that we are dealing with rather complex molecular architectures, which is not effectively accounted in Eq. (1). Something that speaks in this favor is that atomic solids, without any long-range chainlike connectivity, show better agreement between κ and $\kappa^{\min}$ [8]. Additionally, the data in Fig. 6 further suggest that κ is indeed bound by an upper limit of ∼0.4 W/m^{-1}K^{-1} for H-bonded systems resulting from the upper bound of elasticity.

It should also be mentioned that all calculations are performed at k_BT, which is too small to excite high-frequency modes associated with the hydrogen atoms attached to the carbon atoms of different monomers and also the chemically bonded interactions within a chain that often exceed $80\,k_BT$ strength. If all these modes are included in n of Eq. (1), then it will lead to an overestimation of κ. This can, however, be overcome following the treatment proposed in Refs. [19,21] that replaces n by $n_c = 2(n - n_H)/3$ in Eq. (1), with n_H being the density of hydrogen atoms. This also gives an upper classical [Dulong-Petit (DP)] limit of the volumetric heat capacity, $c_{\rm DP} = 3n_ck_B$, and following Eq. (1) gives $\kappa^{\min} = (\pi/432)^{1/3}k_B^{1/3}c^{2/3}(v_\ell + 2v_t)$ [8,19]. In our simulations, we have estimated c using the scaled atomic density n_c and from the energy fluctuation in canonical ensemble, i.e., $c_f = [\langle E^2\rangle - \langle E\rangle^2]/Vk_BT^2$. In Table III we list c for four different polymers where experimental data are available. Reasonably good agreement between c_f, $c_{\rm DP}$, and $c_{\rm exp}$ further suggests that our simulations capture the generic features of κ of commodity plastics.

TABLE III. Volumetric heat capacity c for PMMA, PAP, PAA, and PAM. In simulations, heat capacity is calculated using the energy fluctuations c_f and also the DP values $c_{\rm DP} = 3n_c k_B$. For comparisons, we have also listed available experimental values $c_{\rm exp}$ [19].

Polymer	c_f (MJ/m^{3}K)	$c_{\rm DP}$ (MJ/m^{3}K)	$c_{\rm exp}$ (MJ/m^{3}K)
PMMA	1.40	1.22	1.65
PAP	1.01	1.23	1.67
PAA	1.25	1.84	1.49
PAM	1.50	1.68	1.67

C. Effect of chain stretching on thermal conductivity

As predicted by Eq. (1), if the stiffness of a material is increased, then one also expects to increase κ. This points to a more general design principle of tunability in polymeric plastics. In this work, when we specify an upper bound of κ, we limit our discussion to the standard commodity plastics that are dictated either by the vdW or the H-bond interactions. For zwitterionic polymers or for ionic systems, where long-range electrostatic interactions play a significant role, this upper bound can be increased to a value of $\kappa \sim 0.6$ W/m^{-1}K^{-1} [21]; κ can be even improved further by electrostatic engineering [49,50].

Other studies have also shown that κ can be significantly improved by using stretched polymer configurations that are governed by the phononlike vibrational excitations that are along the covalently bonded polymer backbone. For example, a large body of works have been conducted on fiberlike polymer configurations to enhance κ [32,33,51].

To investigate the effect of polymer stretching, we have made use of a PNIPAM chain with $N_\ell = 256 = 100\,\ell_p$. This chain was previously equilibrated in (good solvent) pure methanol [46]. A typical configuration of an expanded (solvent free) single chain oriented along the z axis is shown in the top panel of Fig. 7. A simulation sample is prepared by placing four expanded chains in a box. This box has an equilibrium z dimension of $L_z = 24.29$ nm at $T = 300$ K, which is comparable to the z component of the end-to-end distance $R_{ez} = 22.32$ nm (see lower panel of Fig. 7). For this system we find $\kappa = 0.70$ Wm^{-1}K^{-1}, i.e., a twofold increase in κ with respect to the bulk value of PNIPAM, see Supplemental Table SI [44]. We have also calculated Young's modulus

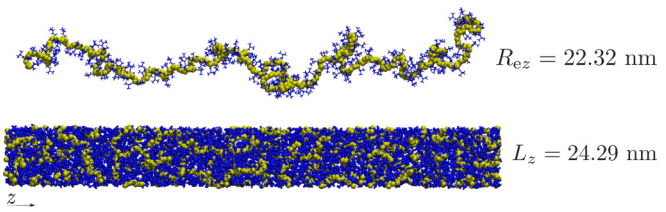

FIG. 7. Simulation snapshot of a fiberlike configuration of dry PNIPAM sample with a chain length $N_\ell = 256$, which corresponds to 100 persistence lengths ℓ_p. Top panel shows a single-chain configuration within the simulation box spanning across the simulation box. Bottom panel shows typical simulation box consisting of four elongated chains. Yellow spheres represent the alkane backbone and the side chains are highlighted in blue.

$E \sim 10$ GPa of the elongated sample. This value is very similar to the bulk data for PNIPAM, see the Supplemental Table SII [44]. The bulklike elasticity of this configuration is not surprising given that even when the individual chains are rather elongated, R_{ez} is only about 1/3 of the total contour length $\ell_c \simeq 60.0$ nm of a PNIPAM chain with $N_\ell = 256$. Therefore, elasticity is not influenced by the bond stretching, rather only by the vdW and H-bond-based nonbonded interactions in a PNIPAM chain.

A closer look at a PNIPAM chain shows that PNIPAM consists of a hydrophobic alkane (PE-like) backbone with hydrophilic side (amide) groups. If this chain is fully stretched along its contour, such that $R_{ez} \simeq \ell_c$, it should also show similar κ values as in the case of single stretched PE, with a reduction because of scattering by the attached side chains. Here, note that for a PE chain with $N_\ell = 256$, $\kappa \simeq 25$ Wm^{-1}K^{-1} [33], which is almost a 40-fold increase from the κ observed for our stretched sample shown in Fig. 7. The increase of κ for stretched configuration is also coupled with the significant increase in the carbon-carbon bond-stretching modulus, which is about $E > 250$ GPa [52].

IV. CONCLUSION

Using large-scale molecular dynamics simulations of all-atom polymer models we investigate thermal transport of commodity plastics and its links to the mechanical response. For this purpose, we have simulated six different linear polymeric materials and one polymer blend with five different mixing ratios [22]. We have investigated the effect of increasing interaction strength, i.e., going from vdW to H bonds [53], on the material stiffness and κ of solid polymeric materials. Our simulation data suggest that there is an upper limit to the achievable κ of commodity plastics, so long as the systems are restricted to vdW and H-bond based plastics. This is because the local and directional nature of H bonds limits the maximum material stiffness between 4.5 and 5.5 GPa, as measured by the shear modulus C_{44}. This upper limit also limits the highest achievable $\kappa \simeq 0.40$ Wm^{-1}K^{-1}. Specific chemical structure and the glass transition temperature T_g are found to play no role in dictating tunability of κ of commodity plastics. We have also investigated the effect of covalent bonds [53] on κ by simulation of a chain oriented polymer configuration. The results presented here are consistent with the minimum thermal conductivity model [8] and existing experimental data [19]. While this work correlates microscopic molecular coordination with elasticity and κ, the concepts presented here may pave ways for the better tunability of the physical properties of the common and smart polymeric materials. Therefore, we expect this to have far-reaching implications in designing environmental friendly materials for advanced functional uses.

ACKNOWLEDGMENTS

D.M. thanks Martin H. Müser, Alireza Nojeh, Daniel Bruns, and Tiago Espinosa de Oliveira for many useful discussions. We further acknowledge support from Compute Canada where simulations were performed. J.R. thanks the Alexander von Humboldt Foundation for financial support.

[1] D. G. Cahill, W. K. Ford, K. E. Goodson, G. D. Mahan, A. Majumdar, H. J. Maris, R. Merlin, and S. R. Phillpot, J Appl. Phys. **93**, 793 (2003).

[2] G. Fugallo and L. Colombo, Phys. Scri. **93**, 043002 (2018).

[3] G. A. Slack, J. Phys. Chem. Solids **34**, 321 (1973).

[4] S. Berber, Y.-K. Kwon, and D. Tomanek, Phys. Rev. Lett. **84**, 4613 (2000).

[5] Z. Fan, L. F. C. Pereira, H.-Q. Wang, J.-C. Zheng, D. Donadio, and A. Harju, Phys. Rev. B **92**, 094301 (2015).

[6] V. Lee, C.-H. Wu, Z.-X. Lou, W.-L. Lee, and C.-W. Chang, Phys. Rev. Lett. **118**, 135901 (2017).

[7] Q.-Y. Li, K. Takahashi, and X. Zhang, Phys. Rev. Lett. **119**, 179601 (2017).

[8] D. G. Cahill, S. K. Watson, and R. O. Pohl, Phys. Rev. B **46**, 6131 (1992).

[9] M. Doi, *Soft Matter Physics* (Oxford University Press, Oxford, 2013).

[10] M. A. Cohen-Stuart, W. T. S. Huck, J. Genzer, M. Müller, C. Ober, M. Stamm, G. B. Sukhorukov, I. Szleifer, V. V. Tsukruk, M. Urban, F. Winnik, S. Zauscher, I. Luzinov, and S. Minko, Nat. Materials **9**, 101 (2010).

[11] D. Mukherji, C. M. Marques, and K. Kremer, Nat. Commun. **5**, 4882 (2014).

[12] S. de Beer, E. Kutnyanszky, P. M. Schön, G. J. Vancso, and M. H. Müser, Nat. Commun. **5**, 3781 (2014).

[13] A. Halperin, M. Kröger, and F. M. Winnik, Angew. Chem. Int. Ed. **54**, 15342 (2015).

[14] Q. R. Zhang and R. Hoogenboom, Prog. Pol. Science **48**, 122 (2015).

[15] D. Mukherji, C. M. Marques, T. Stühn, and K. Kremer, Nat. Commun. **8**, 1374 (2017).

[16] C. L. Choy, Polymer **18**, 984 (1977).

[17] S. Shenogin, A. Bodapati, P. Keblinski, and A. J. H. McGaughey, J Appl. Phys. **105**, 034906 (2009).

[18] G. Kim, D. Lee, A. Shanker, L. Shao, M. S. Kwon, D. Gidley, J. Kim, and K. P. Pipe, Nat. Mat. **14**, 295 (2015).

[19] X. Xie, D. Li, T. Tsai, J. Liu, P. V. Braun, and D. G. Cahill, Macromolecules **49**, 972 (2016).

[20] X. Wei, T. Zhang, and T. Luo, Phys. Chem. Chem. Phys. **18**, 32146 (2016).

[21] X. Xie, K. Yang, D. Li, T.-H. Tsai, J. Shin, P. V. Braun, and D. G. Cahill, Phys. Rev. B **95**, 035406 (2017).

[22] D. Bruns, T. E. de Oliveira, J. Rottler, and D. Mukherji, Macromolecules **52**, 5510 (2019).

[23] B. Qiu and X. Ruan, Phys. Rev. B **80**, 165203 (2009).

[24] W. Shi, Z. Shuai, and D. Wang, Adv. Funct. Mater. **27**, 1702847 (2017).

[25] N. Kim, B. Domercq, S. Yoo, A. Christensen, B. Kippelen, and S. Graham, Appl. Phys. Lett. **87**, 241908 (2005).

[26] M. K. Smith, V. Singh, K. Kalaitzidou, and B. A. Cola, ACS Appl. Mater. Int. **8**, 14788 (2016).

[27] J. Brandrup, E. H. Immergut, and E. A. Grulke (Eds.), *Polymer Handbook*, 4th ed. (Wiley, 2003), Vol. 2.

[28] L. Hu, T. Desai, and P. Keblinski, J. Appl. Phys. **110**, 033517 (2011).

[29] T. Kodama, M. Ohnishi, W. Park, T. Shiga, J. Park, T. Shimada, H. Shinohara, J. Shiomi, and K. E. Goodson, Nat. Mat. **16**, 892 (2017).

[30] C. Mahoney, C. M. Hui, S. Majumdar, Z. Wang, J. A. Malen, M. N. Tchoul, K. Matyjaszewski, and M. R. Bockstaller, Polymer **93**, 72 (2016).

[31] S. Xu, S. Cai, and Z. Liu, ACS Appl. Mater. Int. **10**, 36352 (2018).

[32] A. Henry and G. Chen, Phys. Rev. Lett. **101**, 235502 (2008).

[33] J. Liu and R. Yang, Phys. Rev. B **86**, 104307 (2012).

[34] T. Zhang and T. Luo, ACS Nano **7**, 7592 (2013).

[35] X. Duan, Z. Li, J. Liu, G. Chen, and X. Li, J. Appl. Phys. **125**, 164303 (2019).

[36] S. Pronk, S. Pall, R. Schulz, P. Larsson, P. Bjelkmar, R. Apostolov, M. R. Shirts, J. C. Smith, P. M. Kasson, D. van der Spoel, B. Hess, and E. Lindahl, Bioinformatics **29**, 845 (2013).

[37] S. Plimpton, J Comput. Phys. **117**, 1 (1995).

[38] H. J. C. Berendsen, J. P. M. Postma, W. F. van Gunsteren, A. DiNola, and J. R. Haak, J. Chem. Phys. **81**, 3684 (1984).

[39] U. Essmann, L. Perera, M. L. Berkowitz, T. Darden, H. Lee, and L. G. Pedersen, J. Chem. Phys. **103**, 8577 (1995).

[40] R. W. Hockney, Methods Comput. Phys. **9**, 135 (1970).

[41] B. Hess, H. Bekker, H. J. C. Berendsen, and J. G. E. M. Fraaije, J. Comput. Chem. **18**, 1463 (1997).

[42] T. E. de Oliveira, D. Mukherji, K. Kremer, and P. A. Netz, J. Chem. Phys. **146**, 034904 (2017).

[43] W. L. Jorgensen, D. S. Maxwell, and J. Tirado-Rives, J. Am. Chem. Soc. **118**, 11225 (1996).

[44] See Supplemental Material at http://link.aps.org/supplemental/10.1103/PhysRevMaterials.3.125604 for specific volume as a function of temperature data for different polymers, DSC data for PNIPAM, and table listing elastic moduli and κ of different polymers.

[45] F. Müller-Plathe, J. Chem. Phys. **106**, 6082 (1997).

[46] D. Mukherji, M. Wagner, M. D. Watson, S. Winzen, T. E. de Oliveira, C. M. Marques, and K. Kremer, Soft Matter **12**, 7995 (2016).

[47] W. Tschöp, K. Kremer, J. Batoulis, T. Bürger, and O. Hahn, Acta. Polym. **49**, 61 (1998).

[48] A. Einstein, Ann. Phys. **35**, 679 (1911).

[49] A. Shanker, C. Li, G. Kim, D. Gidley, K. P. Pipe, and J. Kim, Sci. Adv. **3**, e1700342 (2017).

[50] X. Wei and T. Luo, J. Phys. Chem. C **123**, 12659 (2019).

[51] S. Shen, A. Henry, J. Tong, R. Zheng, and G. Chen, Nat. Nanotech. **5**, 251 (2010).

[52] B. Crist and P. G. Herena, J. Polym. Sci. Part B: Polym. Phys. **34**, 449 (1996).

[53] G. P. Desiraju, Acc. Chem. Res. **35**, 565 (2002).